

# Spectroscopic identification of ultranano-crystalline phases within amorphous/nano-crystalline silicon

Mansi Sharma<sup>1,2</sup>, Deepika Chaudhary<sup>1,2</sup>, S. Sudhakar<sup>1</sup>, Preetam Singh<sup>1</sup>, K. M. K. Srivatsa<sup>1,2</sup>, Sushil Kumar<sup>1,2\*</sup>

<sup>1</sup>Network of Institutes for Solar Energy (CSIR-NISE), Physics of Energy Harvesting Division, CSIR – National Physical Laboratory, Dr. K.S. Krishnan Marg, New Delhi 110012, India

<sup>2</sup>Academy of Scientific and Innovative Research (AcSIR), CSIR-NPL Campus, Dr. K.S. Krishnan Marg, New Delhi 110012, India

\*Corresponding author, Tel: (+91) 11-45608650; Fax: (+91) 11-45609310; E-mail: skumar@nplindia.org

Received: 01 February 2016, Revised: 10 May 2016 and Accepted: 22 November 2016

DOI: 10.5185/amlett.2017.6451

www.vbripress.com/aml

## Abstract

The structural transition in accordance to nano sized grain distribution within the amorphous silicon matrix has been described on the basis of spectroscopic analysis as a result of variable input power applied during growth via plasma enhanced chemical vapor deposition (PECVD) process. For this, characterization techniques like micro-ellipsometer, Raman, Field emission Scanning electron microscope (FESEM), and Fourier transform infrared spectroscopy (FTIR) have been effectively utilized to identify transitions in these films particularly in terms of crystallite size (within 1-4 nm) and optical constants. These results indicate that at and above 30 W applied power the separation of two zones takes place as ultranano to nano, leading to the formation of denser matrix having uniformly distributed nano-crystallites. Moreover, these results indicate the presence of unrevealed fine crystallites (ultranano-crystalline phase) as a dominating part of grain boundaries, which may be as ultranano-crystallite phase. The blending of fine nano-crystallites within the amorphous phase might be the possible reason for the formation of nano-crystallites from ultranano-crystallites. Copyright © 2016 VBRI Press.

**Keywords:** PECVD, a/unc/nc-Si:H, spectroscopy ellipsometer.

## Introduction

Since past few decades hydrogenated amorphous silicon (a-Si:H) material has attracted intense scientific interest due to its accessibly remarkable applications in the area of semiconductors especially in photovoltaic industries and flat panel displays in comparison to bulk semiconductors. Its significant advantages such as large area and low process temperature requirements have made it a suitable and affordable alternative for wafer based silicon technology. Despite offering many significant properties, the device performance is limited by its structural disorder which causes the generation of trap centers for carrier recombination in the form of deep level defects [1]. Due to some of such limitations of a-Si:H, present researchers have moved toward the thought of using amorphous silicon based alloys and similar materials with some fraction of crystallinity so called “micro/nano-crystalline silicon ( $\mu\text{c-Si:H/nc-Si:H}$ )” [2]. On the basis of small structural alterations in the conventional a-Si:H the material can further be identified as micro/nano/ultranano-crystalline silicon where distinct physical properties can be observed within the same material due to erratically distributed grains within the amorphous matrix.

As per the suitability of thin film silicon for photovoltaic application, micro/nano-crystalline silicon has come up as an efficient material for the fabrication of existing layers and their possible arrangement in order to have stable and highly efficient solar cell [3]. Hydrogenated nano-crystalline silicon (nc-Si:H) consists of small crystalline grains (< 100 nm) embedded in amorphous silicon (a-Si:H) matrix and has the material band gap about ~ 2.0 eV (higher than a-Si:H band gap) [4]. The presence of these materials is mainly recognized as dispersed heterogeneous phase consisting of voids and dislocations along with the distribution of patchy sized nano-crystallites within the amorphous silicon. This type of structural distribution can alter the specific properties of the material along with the growth and thickness of the film. Since the configuration discrepancy has a strong influence on growth and consequently the device stability as well as efficiency, it is necessary to understand the micro structural formation for the fabrication of device quality nano-crystalline amorphous silicon [5-6]. For the deposition of such thin film amorphous silicon and its alloys PECVD is considered as highly promising technique which favors the uniform growth of high quality material over large area under low processing

temperature conditions [7]. Moreover, the technique offers a great scope for material deposition in terms of structural evolution with the modification in deposition parameters, mainly in terms of pressure, power and dilution. Few reports are available on the investigation of formation of micro/nano-crystalline silicon [8-10] by PECVD technique and the analysis of which were suitably carried out using ellipsometer [11-14]. Amorphous to nano-crystalline phase transition as an influence of high pressure deposition under  $\text{SiH}_4+\text{H}_2+\text{Ar}$  plasma, has been reported by Gope *et al.* [15]. Sanjay K. Ram [16] have reported the effect of hydrogen dilution on the formation of micro-structure and morphology of microcrystalline silicon by PECVD technique using  $\text{SiF}_4$  source gas where the crystallite transition has been identified as a bimodal size distribution. Though various published reports are available to clarify the transition in terms of amorphous and crystalline phases present within the silicon matrix, still the identification of fine nano from the grain boundaries and crystalline phase “whether ultranano-crystallites can be regarded as dominant contribution of grain boundaries or not?” is an open question for the researchers.

The focus of present study is to understand significant structural aspect of nano/ultranano-crystalline silicon in terms of optical constants as observed from ellipsometry analysis, for the nc-Si:H films deposited at different applied RF powers by PECVD technique. Here we have tried to resolve the dielectric spectra in order to identify distinct amorphous and crystalline phases within the material to understand the existence of grain boundaries. For further elucidation of these results, detailed characterizations performed using micro-Raman, FESEM, ellipsometer and infrared spectroscopy.

## Experimental

### Material synthesis

Hydrogenated amorphous/nano-crystalline thin films were deposited on 7059 corning glass and silicon substrates using a capacitively coupled RF 13.56 MHz PECVD reactor at various RF powers applied on 113  $\text{cm}^2$  electrodes. Hydrogen diluted silane (5%  $\text{SiH}_4$  in  $\text{H}_2$ ) was used as precursor gas for plasma generation and substrates were kept at a temperature of 270 °C. During deposition the total gas flow was fixed as 47 sccm (through MKS Mass flow controller) at a deposition pressure of 0.23 Torr (MKS Baratron Digital Gauge meter).

### Characterization

The characterizations of the films were performed on thin films (~ 100 - 200 nm thick) deposited on glass as well on silicon wafer. For detailed optical characterization of the films, ellipsometer studies were carried out using (J. A. Woollam, model: VASE32) for the incident angles 55°, 65° and 75° in the wavelength range 250-1200 nm, from which analysis for spectroscopic parameters for given set of samples was made.

Spectroscopic ellipsometer is considered as most reliable and non-destructive technique for the estimation of the optical properties of thin films including the

thickness, dielectric, refractive index and band gap, where the key principle of spectroscopy is based on the change in polarization of light when travels through the film. The technique is based on theoretical model fitting analysis which is required to overcome the difference between measured and calculated fitting values as a function of photon energy [17]. The experimental fitting for the nc-Si structure has been done using Tauc-Lorentz (TL) and Gaussian-Lorentz model.

The crystalline fraction and the identification of nano-crystallite phases present in the material were probed with the help of Raman spectrometer (InVia Renishaw) using 514 nm  $\text{Ar}^+$  laser. For surface morphology, grain shape and size distribution FESEM was used. Infrared studies were made using Perkin Elmer 2000 spectrometer for the estimation of microstructure parameter and bonded hydrogen content in as deposited films on the basis of infrared active Si-H bonds.

## Results and discussion

The study of various optical phenomena in terms of absorption and reflections due to structural alterations within the thin films has been analyzed by means of spectroscopy ellipsometry where different theoretical models, as mentioned in experimental section, have been employed to have best fit data collection of required parameters for given set of samples. Fig. 1 represents the experimental and model fitted plots of ‘tan  $\psi$ ’ at different incident angles of 55°, 65° and 75° for the films deposited at various applied powers, which evident the precision in the present ellipsometry results.

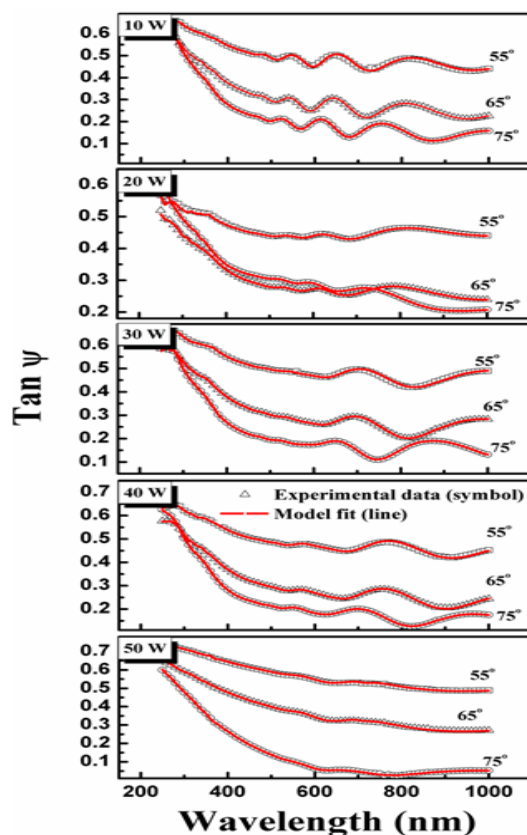


Fig. 1. Experimental and model fitted tan  $\psi$  plots of unc/nc-Si:H films deposited at various applied power at different angle of incidence.

**Table 1.** Various calculated parameters of the unc/nc-Si:H thin films deposited under varying applied power.

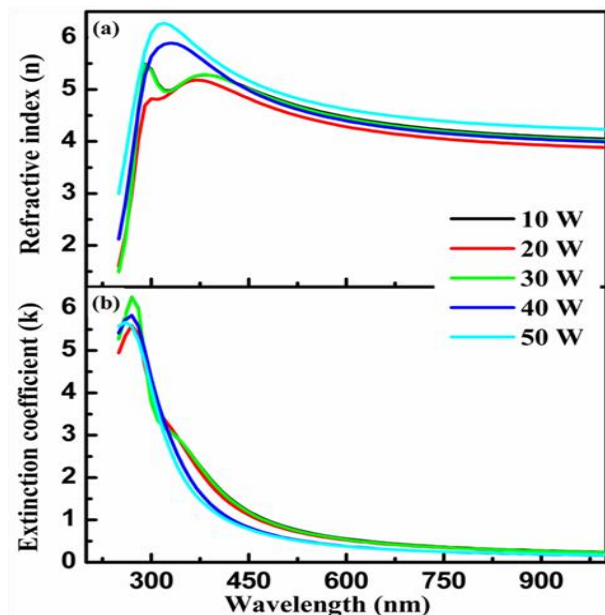
Deposition Power	Deposition Rate (Å/s)	Band gap (eV)	X <sub>c</sub> (%)		X <sub>a</sub> (%)	X <sub>gb</sub> (%)	FT-IR		<ε <sub>2</sub> <sub>max</sub> >	Particle size (nm)	
			Ellipsometer	Raman			C <sub>H</sub> (%)	R		Raman	FESEM
10	0.6	1.9	44	23	20	56	19.2	0.7	6.2	1.8	-
20	0.7	1.9	24	19	33	46	17.5	0.5	1.9	1.6	-
30	0.4	1.9	56	43	15	41	36.8	0.4	6.6	4.8	-
40	0.7	1.9	43	43	22	33	15.8	0.7	5.6	4.5	16
50	0.6	1.9	71	50	16	33	16.2	0.6	15.2	4.3	24

For the clarity of data representation other results were shown for the spectra recorded at incident angle of 75°. The material's absorption analysis was made from the estimated extinction coefficient data from ellipsometer, the inverse relation for this is given as

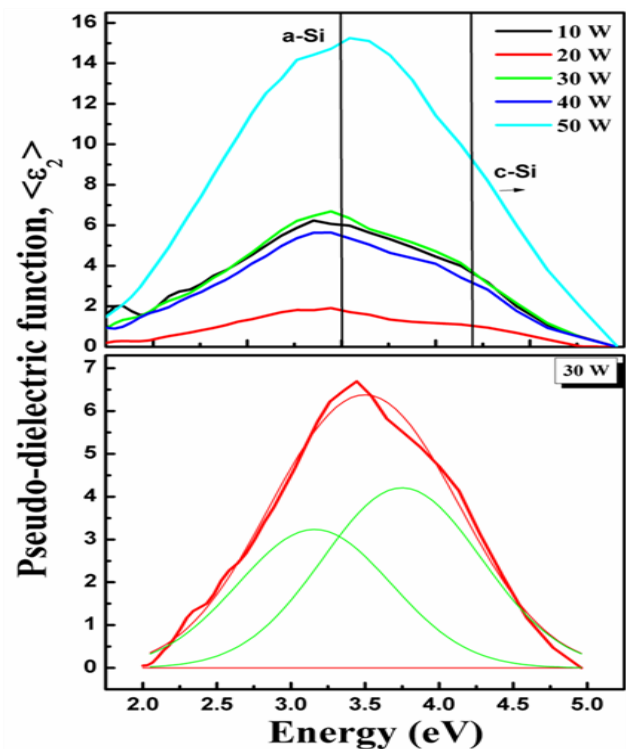
$$\alpha = \frac{4\pi k}{\lambda}$$

where, 'k' is the extinction coefficient of the material and 'α' is the absorption coefficient. From absorption results the band gap was estimated for these films and the values for the same were provided in **Table 1**. These results were supposed to be higher in comparison to the reported band gap of a-Si:H (~ 1.7 – 1.8 eV) and thus signifies the existing nano-crystallites within the amorphous matrix, which were supposed to be responsible for high tunable band gap of the material at different applied RF power.

Moreover, from the results of refractive index and the extinction coefficient from **Fig. 2 (a-b)** it is evident that the material is having transition in terms of the particle size within nm range and their dense distribution which further effects the reflections and light scattering from the material surface. Since the phenomenon of reflection and scattering of light is extremely reliant on the structure and its crystallite arrangement nearer to the surface. Thus, the small variation in the crystallite size can effectively monitor the unwanted reflections, consequently the required scatterings based on the particle size and the compactness of the material matrix can be analyzed.

**Fig. 2.** (a) Refractive index and (b) extinction coefficient measured from ellipsometer for the films deposited at various applied RF power.

**Fig. 3 (a)** represents the pseudo dielectric function <ε<sub>2</sub>> w.r.t photon energy for the given set of mixed phase amorphous and nano-crystalline silicon films deposited at various applied RF powers. Since <ε<sub>2</sub>> itself gives the complete identification of surface, interface and bulk, this parameter has great importance in the complete analyses of the material quality and thus, applicability of the material for photovoltaic. The changes in the value of <ε<sub>2</sub>> in terms of relative spectral shifting can be understood directly via influence of (1) surface roughness (2) density deficits (3) amorphous to crystalline phase transitions [18].

**Fig. 3.** (a) Variation of imaginary pseudo dielectric constant (at incident angle 75o) for the films at various applied RF power and (b) the two peak dissolved spectra for film deposited at 30W.

In view of previous reports the pseudo dielectric spectra is directly related to the density of valence band state and the rising density deficits of the films results in lower <ε<sub>2max</sub>> where the peak position remains same [18]. Additionally, the increase in surface roughness leads to significant reduction in the value of <ε<sub>2max</sub>> and results in peak shifting towards lower photon energy [19]. Also, a significant variation was observed in <ε<sub>2max</sub>> along with the small rising hump towards the high energy. For better understanding and identification of peaks at higher and lower photon energy the spectra was dissolved into two

Gaussian peaks out of which one of the deconvoluted spectra was represented via **Fig. 3(b)** where the two peaks individually corresponds to the crystalline and amorphous phases present in the films. On the basis of this identification the material was found to have more crystalline contribution in terms of high value of  $\langle \epsilon_2 \rangle$  with the increase in applied RF power. The variations in  $\langle \epsilon_{2max} \rangle$  and existing hump are expected due to the distribution of crystallites of distinct sizes within the heterogeneous network of amorphous silicon and on account of which the approximate estimation was also made for the crystalline and amorphous fractions for these samples.

Raman spectroscopy is considered as one of the sensitive tool for structural and phase identification in bulk as well as thin films where the analysis is based on the Raman active phonon vibrations even at room temperature [20-21]. The material recognition can be done on the basis of active Transverse optic (TO), longitudinal optic (LO), transverse acoustic (TA) and longitudinal acoustic (LA) phonon vibration modes. In a-Si all the mentioned modes are Raman active whereas the crystalline silicon will response with the appearance of sharp peak between 520- 522  $\text{cm}^{-1}$  only for the TO mode. Thus, the mixed phase material, where both the phases (amorphous as well crystalline) are supposed to be contributed, will be considered to have a combination of some of active modes (including TO modes) in accordance to dominating phase of the material. **Fig. 4** represents the observed normalized Raman spectra in the range 100 – 800  $\text{cm}^{-1}$  for the given thin films deposited at various applied powers.

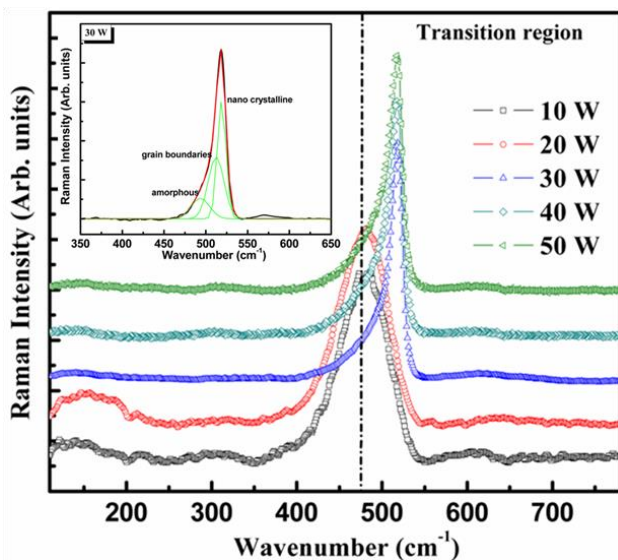


**Fig. 4.** (a) Raman spectra for unc/nc-Si:H films deposited at various applied power (b) three peak dissolved spectra.

From these results it is evident that beyond 20 W power the expected TO peak as commonly observed in case of amorphous or intermediate silicon get shifted from  $\sim 484 \text{ cm}^{-1}$  toward the higher wavenumber at  $\sim 517 \text{ cm}^{-1}$  where the signatures of high crystallinity were predictable which is possibly due to the presence of small crystallites. The estimation for the crystalline fraction was made for the

entire set of sample for which the spectra can be dissolve into three different Gaussian peaks on the basis of this the corresponding equation is given as;

$$X_{nc} \% = \frac{I_c}{I_a + I_{nc} + I_{gb}}, X_{gb} \% = \frac{I_{gb}}{I_a + I_{nc} + I_{gb}} \text{ and } X_a \% = \frac{I_a}{I_a + I_{nc} + I_{gb}} \quad (1)$$

where,  $X_c$ ,  $X_{gb}$  and  $X_a$  are the crystalline, grain boundary and amorphous fraction respectively.  $I_a$ ,  $I_{nc}$  and  $I_{gb}$  represents the integrated area of amorphous, nano-crystalline and grain-boundaries. Here the grain boundaries are supposed to be identified as, in particular, well dissolved phase out of the fine nano-crystallites whose contribution is not deeply distinct of that of crystalline part. The evidence of which can further be scanned on the basis of ellipsometry results where the spectra was dissolved only for two phases. Also, the estimation for the average particle size variation was made using;

$$D_r = 2\pi \sqrt{\frac{B}{\Delta w}} \quad (2)$$

where,  $\Delta w$  is the wavenumber shift correspond to the nano-crystalline peak reference to the crystalline peak i.e.  $522 \text{ cm}^{-1}$  and  $B = 2.24 \text{ nm}^2 \text{ cm}^{-1}$  for silicon [22]. A significant change in the particle distribution and accordingly the material crystallinity was observed with the increase in applied power which leads to conclude the presence of bigger crystallites in high power plasma environment which reflects the significant contribution of higher silane radicals and hydrogen flux in support of the controlled plasma reactions. These observations can be well understood in terms of material phase transition where the transition results in creation of nano from ultranano-crystalline silicon. Clustering of ultranano-crystallites within the amorphous phase might be the possible reason for the nano-crystalline growth. Raman results are found to be in correlation with the results of  $X_c$  observed from ellipsometer. The nano-crystallite distribution in terms of crystalline volume fraction from ellipsometer along with the amorphous and fine nano-crystalline contribution as estimated from Raman spectra is given in **Table 1**. From **Table 1** it can be observed that initially for the sample deposited at 10 W the crystalline fraction is high for compared to 20 W applied RF which could possibly be related to the high grain boundary contribution instead of the higher amorphous content. Thus, the material deposited under these conditions has more voids as well as the high structural disorder which may also participate as an obligatory error in estimation of exact crystalline content for the same. For the depositions at and above 30 W power the crystalline fraction was found to increase up to  $\sim 50\%$  on the basis of Raman spectra and  $\sim 70\%$  as estimated from dielectric spectra which could further consider in terms of lesser boundaries and accordingly the amorphous content along with the effective variation in the crystallite size. Further, the visible discrepancy in the results of crystalline fraction estimated from both the spectroscopy techniques can be

understood in terms of the well-defined region for grain boundaries in Raman spectra which were not alienated out in dielectric spectra. In view of the results so far observed from ellipsometry and Raman one may suggest that the grain boundaries are not alienated from the ultranano-crystalline phase.

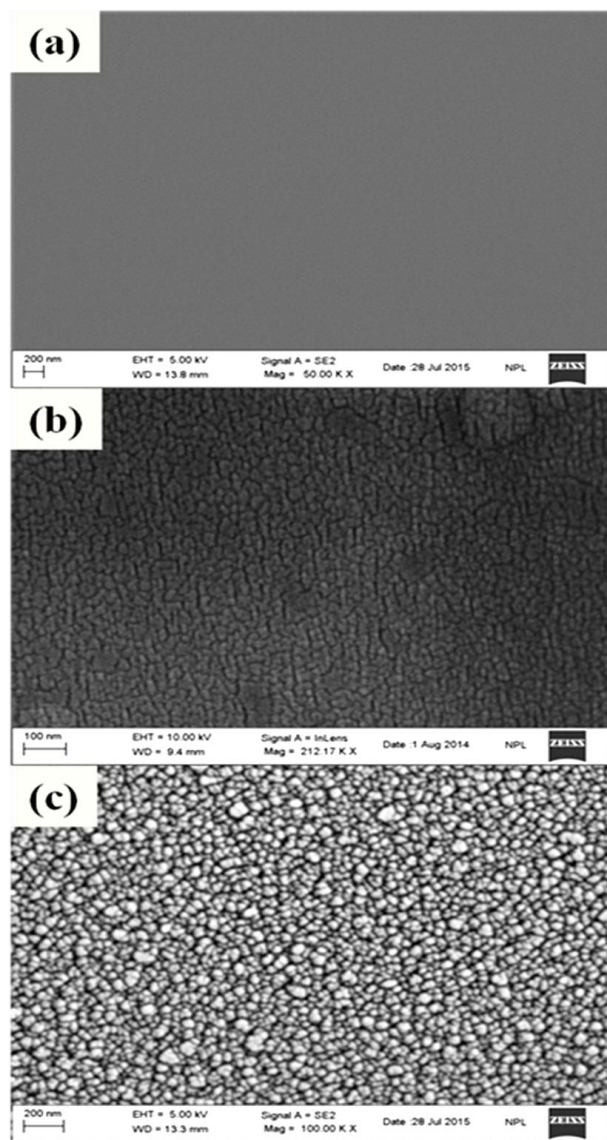


**Fig. 5.** SEM micrograph for grain distribution for the films deposited at (a) 10 W (b) 40 W and (c) 50 W applied power.

**Fig 5 (a-c)** depicts the scanning electron (SEM) micrograph of the films deposited at 10 W, 40 W and 50 W RF power. From the SEM results for deposition under high power plasma (40 W and 50 W) the material was found to have uniformly distributed crystals with well-defined grain boundaries which were observed to form a highly dense matrix of nano-crystallites diluted within the amorphous phase. On the other hand, at low applied power (10 W) the material was observed to be entirely in amorphous nature with no specified grain distribution. This observation for the structural transitions under different zones of deposition power was probably due to the high ion energy and ion flux which strongly influence the growth of nano-crystalline during

deposition. At high power the energetic ions and their impingement rate directly favors the condition for growth of nano-crystalline material whereas at low power the possibilities of these alteration in the structure were very minimal. These results were best correlated with the above mentioned results of transition observed from Raman and absorption curves which signify the variation of nano particle within the amorphous matrix where the change observed in their crystalline fraction as moving towards high power growth regime.

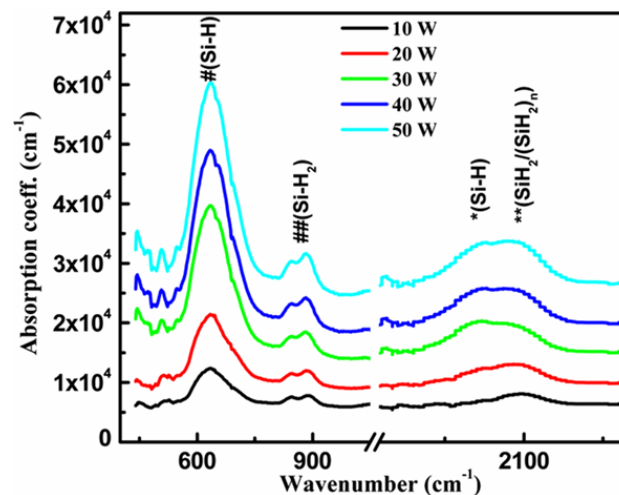


**Fig. 6.** FTIR spectra for the films deposited at various applied power # Wagging band, ## Bending band, \*Symmetric stretch, \*\*Asymmetric stretch.

Fourier transform infrared spectroscopy (FTIR) in case of amorphous and micro/nano crystalline silicon thin films is commonly used to identify the present bonding configuration and the estimation of hydrogen content with the help of their corresponding vibration modes. The infrared absorption spectra for a-Si/nc/ $\mu$ c-Si:H is composed of combination of different modes of IR active vibrations which mainly include the wagging band ( $600\text{--}700\text{ cm}^{-1}$ ) of SiH, bending modes ( $770\text{--}920\text{ cm}^{-1}$ ) of SiH<sub>2</sub>, (SiH<sub>2</sub>)<sub>n</sub> and stretching modes of vibration ( $1900\text{--}2000\text{ cm}^{-1}$ ) of SiH, SiH<sub>2</sub> and (SiH<sub>2</sub>)<sub>n</sub> [23]. **Fig. 6** shows the FTIR absorption spectra for the films deposited at various RF power. In accordance to previous reports, the spectra can further be deconvoluted into two broad Gaussian peaks centered around  $\sim 2000\text{ cm}^{-1}$  and  $\sim 2100\text{ cm}^{-1}$  which corresponds to stretching vibrations of SiH and SiH<sub>2</sub>, (SiH<sub>2</sub>)<sub>n</sub> respectively [24] to identify the nano-crystallites vibration. Here from the precise observation of corresponding stretching modes after deconvolution for the same, it was found that initially at 10 W and 20 W the stretching modes was almost centered nearer to  $2100\text{ cm}^{-1}$ . This peak shifting corresponds to the clustered SiH at grain boundaries and can also be correlated with the results of the grain boundary volume fraction as observed from Raman spectra. As the power increases further, the boundaries start getting diluted with the existing crystallites which then results in the broadening of peaks correspond to stretching vibrations. Moreover, the intensity of bending modes of vibration was found to increase for the films deposited at and beyond 30 W. This rise in intensity is attributed to the rising density of higher

silane i.e SiH<sub>2</sub> and (SiH<sub>2</sub>)<sub>n</sub> the excess of which may leads to the formation of defects along with the nc/μc formation [10]. The microstructure changes in the films can also be responsible for the observable shift in the FTIR peaks. The estimation of microstructure parameter was made (for stretching bands) to study the structural transitions.

$R^* = \frac{I_{2070-2100}}{I_{2070-2100} + I_{2000}}$  is the microstructure parameter, typical values of which correspond to a roundabout measurement for the presence of higher order silane radical within the film. For the given set of samples the value  $R^*$  was found to lie in range of 0.43 - 0.79. High microstructure parameter corresponds to more SiH<sub>2</sub> bonding instead of SiH which evident the dominating phase of clustered hydrogen bonding in the films as well the material porosity is directly related to the density of such bonds the presence of which should be evade during growth in order to have a stable device quality material.

The calculation for bonded hydrogen content via wagging band has been made by using the formula:

$$C_H = [A_{\omega} \left( \int_{-\infty}^{+\infty} \frac{\alpha(\omega)}{\omega} d\omega / N_{Si} \right) * 100] \% \quad (3)$$

where  $\alpha(\omega)$  is the absorption coefficient and is defined in equation (4),  $\omega$  is the wavenumber in cm<sup>-1</sup>,  $A_{\omega}$  is the oscillator strength,  $A_{640} = 2.1 \times 10^{19}$  cm<sup>-2</sup> & and  $N_{Si}$  is the atomic density of crystalline silicon is  $5 \times 10^{22}$  cm<sup>-3</sup> [25-27]. The value of absorption coefficient was estimated from the transmission data using equation (4) which is given as:

$$\alpha(\omega) = \frac{\ln(XR) - \ln(\sqrt{1+X^2} - 1)}{d} \quad (4)$$

where the constants are given as;  $X = \frac{2R(T/T_0)}{1-R^2}$ , here R is the reflectivity of silicon (R = 0.3 for silicon) [28].

The variation of hydrogen content and the typical values of  $R^*$  parameter of films with the applied RF power are given in Table.1 in order to have their specific correlation with the results of Raman and ellipsometer. Here the existing high hydrogen content elucidates the widening of material band gap which was already marked from the absorption results. On account of the results of ellipsometry, Raman, lowest  $R^*$  (0.4) and the typical higher value of bonded hydrogen content in the film deposited at 30 W reveals the initialization of the phase transformation in terms of fine nano-crystallites. Thus, 30 W power is considered as the point of onset of crystallinity where the higher hydrogen and the low microstructure parameter may corresponds to the material phase where the boundaries are on verge of relaxation and thus unevenly settled and dense matrix offer more hydrogen to get bonded with silicon instead of Si - Si bond. Beyond this the particles get transformed and attain comparatively bigger size, which further restricts the passivation of boundaries resulting in clustered hydrogen bonding configuration. Our results indicate that the material shows transition in terms of crystallite size beyond 30 W power, also the grain boundaries amalgamate due to formation of bigger crystals due to

which there is improvement in the surface density with the reduction in voids and vacancies [29]. It is explicable here that the films deposited at high applied RF power (> 30 W) may result in the structure having denser network of uniformly distributed bigger size grains. The understanding of such fine tuning of nano-crystallites opens up a wide scope for material applicability not only in photovoltaic's but also to other devices like thin film transistor (TFT), anti-reflection coatings, non-volatile memory devices [30-31]. Explicitly if a case for anti-reflecting coating for solar cell is considered the exiting crystallites would effectively controls the unwanted reflection, thus improves the device performance.

## Conclusion

nc/μc-Si:H thin films were deposited using conventional RF PECVD technique at various applied powers. Structural and optical characterizations revealed that at 30 W of applied power sudden change occurs in crystallite size (1.6 - 1.8 nm to 4.3 - 4.8 nm) and optical constants, indicating that the separation of two zones takes place as ultranano to nano, leading to the formation of denser matrix having uniformly distributed nano-crystallites. These results suggest the presence of crystalline phase out of the grain boundary where the foremost contribution of boundaries is the ultranano-crystallite silicon. Therefore, the grain boundaries can be regarded as molten crystalline phase whose dominate contribution may alter the film properties. These findings will help to understand the effective way to have control over the fine structural transition and their analysis, and thereby designing efficient p-i-n layers for thin film silicon solar cell applications including multi-junction/hetero-junction/hetero-junction with intrinsic layer.

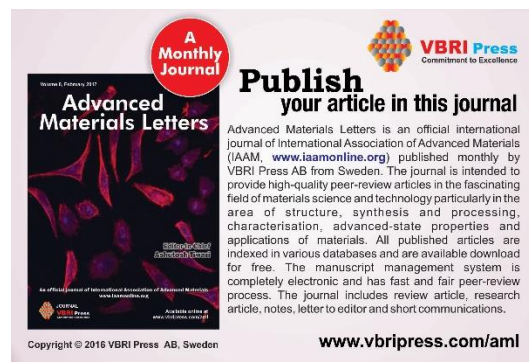
## Acknowledgements

The authors are grateful to Director, CSIR National Physical Laboratory, New Delhi (India) for his kind support. We are also thankful to Dr. Bhanu Pratap Singh, Dr. S. K. Dhawan and Dr. Ajay Dhar from NPL, New Delhi for providing Raman Spectroscopy, FTIR and FESEM facilities respectively. As well the authors are thankful to Ms Kalpana Lodhi from NPL for providing help during experimentation. We also acknowledge CSIR-India for TAPSUN program and MNRE, Govt. of India for the research grant (sanction 31/29/2010-11/PVSE).

## References

- Street, R.A.; Hydrogenated amorphous silicon. *Cambridge University Press*. 2005.
- Shah, AV.; Meier, J.; Vallat-Sauvain, E.; Wyrsh, N.; Kroll, U.; Droz, C.; & Graf, U. *Sol. Energy Mater. Sol. Cells*. 2003, 78, 469. DOI: [10.1016/S0927-0248\(02\)00448-8](https://doi.org/10.1016/S0927-0248(02)00448-8)
- Ballif, C.; Bailat, J.; Domine, D.; Steinhäuser, J.; Fay, S.; Python, M.; & Feitknecht, L. *21<sup>th</sup> European Photovoltaic Solar Energy Conference and Exhibition*, Dresden. 2006.
- Singh, V.; Tiwari, A.; Pandey, S.; Singh, S. K.; Sanghi, R.; *Journal of Applied Polymer Science*, 2007, 104, 536. DOI: [10.1002/app.25585](https://doi.org/10.1002/app.25585)
- Goerlitz, M.; Beck, N.; Torres, P.; Kroll, U.; Keppner, H.; Meier, J.; Koehler, J.; Wyrsh, N & Shah, AV. *MRS Proceedings*. 1997, 467, 301. DOI: [10.1557/PROC-467-301](https://doi.org/10.1557/PROC-467-301).
- Yan, B.; Yue, G.; Owens, JM.; Yang, J.; Guha, S. *Appl. Phys Lett*. 2004, 85, 1925.

- DOI: [10.1063/1.1790072](https://doi.org/10.1063/1.1790072)
7. Tanaka, H & Inokuti, M. *Advances In Atomic, Molecular, and Optical Physics*. **2000**, 43, 1.  
DOI: [10.1016/S1049-250X\(08\)60120-2](https://doi.org/10.1016/S1049-250X(08)60120-2)
8. Matsuda, A. *J Non-Crystal. Solids*. **2004**, 338, 1.  
DOI: [10.1016/j.jnoncrysol.2004.02.012](https://doi.org/10.1016/j.jnoncrysol.2004.02.012)
9. Mahan, AH.; Yang, J.; Guha, S & Williamson, DL. *Phys. Review B*. **2000**, 61, 1677.  
DOI: [10.1103/PhysRevB.61.1677](https://doi.org/10.1103/PhysRevB.61.1677)
10. Gope, J.; Kumar, S.; Singh, S.; Rauthan, CMS & Srivastava, PC. *Silicon*. **2012**, 4, 127.  
DOI: [10.1007/s12633-012-9109-z](https://doi.org/10.1007/s12633-012-9109-z)
11. Fujiwara, H.; Kondo, M & Matsuda, A. *Phys. Rev. B*. **2001**, 63, 115306.  
DOI: [10.1103/PhysRevB.63.115306](https://doi.org/10.1103/PhysRevB.63.115306)
12. Chakraborty, K & Das, D. *Sol. Energy Mater. Sol. Cells*. **2006**, 90, 849.  
DOI: [10.1016/j.solmat.2005.05.004](https://doi.org/10.1016/j.solmat.2005.05.004)
13. Amans, D.; Callard, S.; Gagnaire, A.; Joseph, J.; Ledoux, G.; & Huisken, F. *J. Appl. Phys.* **2003**, 93, 4173.  
DOI: [10.1063/1.1538344](https://doi.org/10.1063/1.1538344)
14. Jellison Jr, GE.; Chisholm, MF & Gorbatkin, SM. *Appl. Phys. Lett.* 1993, 62, 3348.  
DOI: [10.1063/1.109067](https://doi.org/10.1063/1.109067)
15. Gope, J.; Kumar, S.; Parashar, A., Dixit, PN.; Rauthan, CMS.; Panwar, OS.; Patel DN & Aggarwal, SC. *J Non-Crystal. Solids*. **2009**, 355, 2228.  
DOI: [10.1016/j.jnoncrysol.2009.07.013](https://doi.org/10.1016/j.jnoncrysol.2009.07.013)
16. Ram, SK.; Islam, MN.; i Cabarrocas, PR.; & Kumar, S. *Thin Solid Films*. **2008**, 516, 6863.  
DOI: [10.1016/j.tsf.2007.12.113](https://doi.org/10.1016/j.tsf.2007.12.113)
17. Herzinger, CM.; Johs, B.; McGahan, WA.; Woollam, JA.; Paulson, W. *J Appl. Phys.* **1998**, 83, 3323.  
DOI: [10.1063/1.367101](https://doi.org/10.1063/1.367101)
18. Giri, PK.; Tripurasundari, S.; Raghavan, G.; Panigrahi, BK.; Magudapathy, P.; Nair, KGM.; Tyagi, AK. *J. Appl. Phys.* 2001, 90, 659.  
DOI: [10.1063/1.1379055](https://doi.org/10.1063/1.1379055)
19. Dixit, PN.; Panwar, OS.; Satyanarayan, BS.; Bhattacharyya, R. *Sol. Energy Mater Sol. Cells*, **1995**, 37, 143.  
DOI: [10.1016/0927-0248\(94\)00203-7](https://doi.org/10.1016/0927-0248(94)00203-7)
20. Han, D.; Lorentzen, JD.; Weinberg-Wolf, J.; McNeil, LE & Wang, Q. *J Appl. Phys.* **2003**, 94, 2930.  
DOI: [10.1063/1.1598298](https://doi.org/10.1063/1.1598298)
21. Vink, RLC.; Barkema, GT.; Van Der Weg, WF. *Phys. Rev. B*, **2001**, 63, 115210.  
DOI: [10.1103/PhysRevB.63.115210](https://doi.org/10.1103/PhysRevB.63.115210)
22. Edelberg, E.; Bergh, S.; Naone, R.; Hall, M.; Aydil, ES.. *J. Appl. Phys.* **1997**, 81, 2410.  
DOI: [10.1063/1.364247](https://doi.org/10.1063/1.364247)
23. Gope, J.; Kumar, S.; Sudhakar, S.; Rauthan, CMS.; Srivastava, PC. *Mater. Chem. Phys*, **2013**, 141, 89.  
DOI: [10.1016/j.matchemphys.2013.04.028](https://doi.org/10.1016/j.matchemphys.2013.04.028)
24. Tsu, DV.; Lucovsky, G.; Davidson, BN. *Phys. Rev. B*. **1989**, 40, 1795.  
DOI: [10.1103/PhysRevB.40.1795](https://doi.org/10.1103/PhysRevB.40.1795)
25. Brodsky, MH.; Cardona M.; Cuomo, JJ. *Phys. Rev. B*. 1977, 16, 3556.  
DOI: [10.1103/PhysRevB.16.3556](https://doi.org/10.1103/PhysRevB.16.3556)
26. Langford, AA.; Fleet, ML.; Nelson, BP.; Lanford, WA.; Maley, N. *Phys. Rev. B*. 1992, 45, 13367.  
DOI: [10.1103/PhysRevB.45.13367](https://doi.org/10.1103/PhysRevB.45.13367)
27. Chaudhary, D.; Sharma, M.; Sudhakar, S.; Kumar, S. *Silicon*. 2015(accepted).  
DOI: [10.1007/s12633-015-9374-8](https://doi.org/10.1007/s12633-015-9374-8)
28. Manfredotti, C.; Fizzotti, F.; Boero, M.; Pastorino, P.; Polesello, P.; Vittone, E. *Phys. Rev. B*. 1994 50, 18046.  
DOI: [10.1103/PhysRevB.50.18046](https://doi.org/10.1103/PhysRevB.50.18046)
29. Smets, AHM.; Kessels, WMM.; Van de Sanden, MCM. *Appl. Phys. Lett.* **2003**, 82, 1547.  
DOI: [10.1063/1.1559657](https://doi.org/10.1063/1.1559657)
30. Cheng, IC.; Wagner, S. *IEEE Proceedings* **2003**, 150, 339. IET.  
DOI: [10.1049/ip-cds:20030573](https://doi.org/10.1049/ip-cds:20030573)
31. Jung, S.; Yi, J. *Elec. Deice. Lett. IEEE*, 31, 981  
DOI: [10.1109/LED.2010.2053192](https://doi.org/10.1109/LED.2010.2053192)



**A Monthly Journal**

**Publish your article in this journal**

Advanced Materials Letters is an official international journal of International Association of Advanced Materials (IAAM, [www.iaamonline.org](http://www.iaamonline.org)) published monthly by VBRI Press AB from Sweden. The journal is intended to provide high-quality peer-review articles in the fascinating field of materials science and technology particularly in the area of structure, synthesis and processing, characterisation, advanced-state properties and applications of materials. All published articles are indexed in various databases and are available download for free. The manuscript management system is completely electronic and has fast and fair peer-review process. The journal includes review article, research article, notes, letter to editor and short communications.

Copyright © 2016 VBRI Press AB, Sweden

[www.vbripress.com/aml](http://www.vbripress.com/aml)